Journal of Energetic Materials
Publication details, including instructions for authors and subscription information:
http://www.informaworld.com/smpp/title~content=t713770432

Computer molecular dynamics of 2-d water (ice) structures under shock by

Paul Harris[a]; Arnold M. Karo[b]
[a] US Army Armament, Munitions and Chemical Command Dover, New Jersey [b] Lawrence Livermore National Laboratory, Livermore, California

To cite this Article Harris, Paul and Karo, Arnold M.(1985) 'Computer molecular dynamics of 2-d water (ice) structures under shock by', Journal of Energetic Materials, 3: 1, 1 — 33
To link to this Article: DOI: 10.1080/07370658508221233
URL: http://dx.doi.org/10.1080/07370658508221233

COMPUTER MOLECULAR DYNAMICS OF 2-D WATER (ICE) STRUCTURES UNDER SHOCK

by

Paul Harris
US Army Armament, Munitions and Chemical Command
Dover, New Jersey 07801-5001

Arnold M. Karo
Lawrence Livermore National Laboratory
Livermore, California 94550

ABSTRACT

Computer molecular dynamics has been used to study the shock-front transition region for a series of two-dimensional hydrogen-bonded structures composed of water-vapor molecules. Two different structures were examined and different intermolecular potentials were considered. Sample sizes and running times were chosen to correspond to the predicted shock-front rise-time in real water. In this way, the effect of different potentials and initial structures on the equilibration associated with the shock-front transition in water could be investigated. In addition to studying the development and incipient relaxation of shock-polarization states, we have also considered the propagation and possible incipient

Journal of Energetic Materials vol. 3, 1-33 (1985)

Published in 1985 by Dowden, Brodman & Devine, Inc.

relaxation of structural phase transitions occurring in two-dimensional structures. The results of these molecular dynamics calculations are compared with the experimental shock behavior of real water; in particular, comparisons are made with respect to intermolecular hydrogen-bond breaking, dissociation and dissociation-related electrical conductivity data.

INTRODUCTION

The problem of providing a detailed (although averaged) description of molecular behavior within a shock-front transition region is of both academic and applied interest. The academic interest is that, except for the case of a condensed monatomic noble gas[1-4], the problem has never been successfully treated for realistic condensed molecular media. The applied interest is mostly connected to understanding the possibility of enhanced chemistry occuring within the high-strain-rate shock-front region.

Water was chosen for this study because water has been extensively studied both macroscopically and microscopically; because shock-polarization[5,6] and shock-front optical reflectivity[7] data exist for water; and because, to a first approximation, each molecule could, if desired for purposes of simplicity, be considered as a rigid structure in the presence of an intermolecular potential. Thus, water should represent

a benchmark test of the ability of computer molecular dynamics (CMD) to predict the known shock-wave properties of a realistic and interesting material.

The work to be described in this report represents the steps along the road to a full and accurate CMD study of shocked water. Two different initial two-dimensional (2D) structures were run. One of these structures was then also run with important changes in the intermolecular potentials. The problems were run only in 2D configurations because the most important aspect of the physics (chemistry) of water is that associated with the intermolecular hydrogen bonding, which can be adequately represented in 2D, and to save time (as well as expense) during the actual computations. In our calculations we have not found it necessary to treat the water molecular as rigid and have therefore allowed for all 2D molecular degrees of freedom.

Among the shock-related phenomena studied were the propagation and possible commencement of relaxation of structural phase transitions, the development and possible commencement of relaxation of shock-polarization states, and the importance of the details of the potentials to the general questions of realistic shock wave CMD.

For these studies, the largest impacted sample considered was composed of 4 x 20 water molecules (20 molecules in the

direction of shock propagation), and the longest running time (measured from impact) was 0.65 picoseconds. These sample length and run times correspond approximately to the predicted[5] shock-front rise time in real water of approximately one picosecond. Thus, at least in principle, the effect of potentials and initial structures upon the equilibration associated with the shock-front transition in water could begin to be investigated with the CMD techniques presented in this report.

This report presents results only for impact velocities of 0.75 Å per tick[+] (or 7.5 x 10^5 cm/sec) and 0.4 Å per tick. Such impact velocities represent (for real 3-dimensional water under 1-dimensional strain with symmetric impact) pressures of approximately 300 kbar (or 30 GPa) and 100 kbar, respectively[9].

The electrical conductivity of water is known from experiments[10] to saturate at shock pressures above 300 kbar. It would thus seem possible to characterize real water above 300 kbar as being entirely ionized. Ionized water has been described as consisting primarily of protonated water complexes[11] (e.g., $H_9O_4^+$) and hydroxide ions. In so far as such protonated complexes or hydroxide radicals were not observed (i.e., no recognizable "dissociation"), the simple

[+] One "tick" is 10 femtoseconds or 10^{-14} sec - a convenient time in CMD (10^{-14} sec is approximately one H_2 vibrational period).

CMD model we have employed clearly requires additional refinement in order to be in agreement with this probable picture. Thus, at this moment, although it is not completely clear what the difficulty is, an improved model must include the effective pressure or density dependence of the potential barrier to proton transfer. Such a pressure dependence could easily appear via the influence of neighboring molecules on an otherwise isolated intermolecular hydrogen bond. It appears that, although the shock contains sufficient energy to overcome the original tetrahedral orientation and average bonding configuration of the water molecular lattice (as discussed in the following sections), because of the absence of energetically low-lying pathways that energy is not being transferred during the time of our simulation studies in such a way as to yield proton transfer and the formation of complex ionic species. (In our view, the lack of observed complex formation at the 0.75 Å/tick impact velocity indicates clearly a direction for further study).

With the exception of the intermolecular hydrogen-hydrogen interactions, all of the interatomic potentials employed were of the Morse type (with a cut-off distance and damping factor). Some of the intermolecular hydrogen-hydrogen potentials were chosen to be Coulomb-like (based upon the molecular orbital hydrogen-bond studies of Morokuma and Pedersen[12]).

The above-mentioned choice of intermolecular potentials describes, firstly, a relatively fixed (i.e., a steep-sided moderately-shallow potential well) OH bond distance of $\sim$1.76 Å. Secondly, the choice describes the separation of water molecules which are hydrogen bonded to a common oxygen atom. That second point leads to a very shallow and gradually sloping OO potential well yielding a nearest-neighbor OO distance of $\sim$2.76 Å.

With the above OH and OO intermolecular potentials, together with a reasonable description of the water-vapor molecular, it is not necessary to require a potential well for the HH intermolecular interaction because the basic water structure (in the sense of an ice) is approximately fixed. Accordingly, either a Coulomb or Morse type of interaction can be chosen for the intermolecular HH interaction. This choice allows for a parameter (charge in the case of the Coulomb interaction) which, when varied, will have an influence upon the ease of rotation of one water molecule in the field of another. The rotational-influence point-of-view is also in keeping with our desire to ultimately correlate the CMD work with existing shock-polarization data[5,6] (shock polarization is intimately connected to the shock-induced average rotation of the water molecular electric dipole moment).

The CMD calculations were carried out with initially quiescent (T = 0 degree Kelvin) lattices. The basic reason for the T = 0 K choice is that for a Hugoniot pressure of ∿300 kbar the shock-induced temperature change (∿2000 K) is so large compared to room temperature that it is not likely that an initial temperature of ∿300 K could have any effect upon the qualitative results being investigated here. With that understanding, any initial thermalization of the lattice would have represented an unnecessary expenditure of time and money for these first-step calculations.

All of the CMD problems were run with periodic boundary[13] conditions in the direction transverse to the direction of shock propagation. This means that if an atom is at position (x, y), then there are also identically behaving atoms at positions (x, y + nL) for all integer n where L is the transverse sample dimension "size". To insure basic structural stability, each sample (with related potentials) was "run" without periodic boundary conditions (in the absence of impact). No phase transitions were noted in those stability tests, and where internal heating occurred due to small initial intrinsic strain, that heating was always correctable by reducing the error in the initial atomic equilibrium positions.

SOME PRELIMINARY NUMBERS

Before proceeding with the detailed presentation of the actual potentials and structures employed in these CMD calculations, it is worthwhile to discuss some order-of-magnitude numbers relating to real water and its behavior under shock.

A. An average value for the water-vapor dissociation energy (removal of one hydrogen) is approximately 120 kcal/mole or 8.33×10^{-12} ergs/molecule.

B. The symmetrical bending mode for a water-vapor molecule has a characteristic frequency[14] f of approximately 1600 cm^{-1}. For a spring constant K given by $K = m_H (2\pi f)^2$ with m_H being a hydrogen mass, there is an associated bending energy of $E = 0.5\ K\ (\Delta X)^2$, where ΔX is the hydrogen-hydrogen vibrational amplitude. It can be seen that a (ΔX) value of 0.2 Å corresponds to approximately 3×10^{-13} ergs.

C. The hydrogen-bond (intermolecular) energy responsible for the basic structure of water and ice is[15] approximately 5 kcal/mole or 3.4×10^{-13} ergs/molecule.

D. At 10 kbar, each water molecule acquires a particle (flow) velocity (4.26×10^4 cm/sec) kinetic energy of $0.5\ m_{H_2O} u_p^2$ or 2.6×10^{14} ergs. m_{H_2O} is the water-vapor molecular mass and u_p the particle velocity. There is also a PdV contribution (for a 20% strain[9])

of approximately the same energy per molecule. The water temperature is raised[9] approximately 34 K to 327 K so that after equilibration each degree of freedom is characterized by a thermal energy of 0.5 kT or 2.4×10^{-14} erg.

E. At 100 kbar, the flow and PdV contributions per molecule are each approximately 5.7×10^{-13} ergs while each degree of freedom is characterized by 843 K or 5.8×10^{-14} erg.

F. At 300 kbar, the flow and PdV contributions per molecule are each approximately 2.2×10^{-12} ergs while each degree of freedom is characterized by 2310 K or 1.5×10^{-13} erg.

From A through F above, the following is to be expected with increasing shock pressure. At 10 kbar, neither intermolecular OH bond breaking, intramolecular HH separation changes, or dissociation should occur. At 100 kbar, intermolecular OH bond breaking and changes in HH intermolecular separation should occur, but there should not be any water-vapor molecule dissociation. The 100 kbar expectations also hold at 300 kbar.

What is seen in the CMD runs to be discussed below is intermolecular OH bond breaking and intermolecular HH separation distance changes at 100 kbar and above. In accordance with the binding energies associated with the potentials we are using,

no water-vapor molecule dissociation is seen. Thus, with the exception of the previously-discussed ionization via proton transfer interpretation of the experimental electrical conductivity saturation near 300 kbar, the CMD runs are behaving as desired.

Thus, the various intermolecular and intramolecular energies are a benchmark not only for the potentials to be described in the next section but also a benchmark for the consequent behavior of the shocked CMD water structures.

THE POTENTIALS AND STRUCTURES

With the exception of the HH intermolecular potentials, all of the potentials employed were of the Morse type:

$$V(R) = D_e \left[e^{-A_1(R-R_e)} - 1 \right]^2 \qquad (1)$$

where

R_e = The equilibrium interatomic separation [where V(R) achieves a minimum].

$-D_e$ = The energy of the potential minimum relative to V (∞).

A_1 = The small displacement (relative to R_e) force constant parameter with the small displacement force given by $-2D_eA_1^2(R-R_e)$.

The HH intermolecular potentials were either of the Morse type, Eq. (1), or the Coulomb type, given by

$$V(R) = \alpha \frac{Q^2}{R} \qquad (2)$$

where

α = The attraction-repulsion parameter. $\alpha = +1$ for repulsion or -1 for attraction.

Q = The interaction strength.

Table 1 gives a summary of the three CMD runs to be presented in this report in terms of intermolecular potentials, impact velocities, and the starting lattice structures. Figures 1 and 2 illustrate the two starting structures (henceforth called triangular and square, respectively) with the related initial distances and angles.

TABLE 1

SUMMARY OF WATER IMPACT CONFIGURATIONS

RUN NUMBER*	STARTING LATTICE STRUCTURE	IMPACT VELOCITY (cm/sec)	INTERMOLECULAR POTENTIALS H-H	O-H	O-O
1 (F3H20B)	TRIANGULAR	7.5×10^5	MORSE	MORSE	MORSE
2 (F3DF2C)	TRIANGULAR	7.5×10^5	REPULSIVE COULOMB	MORSE	MORSE
3 (F3SQUA)	SQUARE	4.0×10^5	REPULSIVE COULOMB	MORSE	MORSE

*The values in parentheses are for the authors' internal bookkeeping purposes.

Aside from the difference in unit-cell configurations between the two starting structures (and a corresponding compressibility difference), the lattices are characterized by different responses to local rotation because of the different hydrogen arrangements and the associated intermolecular HH potentials. Such rotational response differences are important to the question of shock polarization.

With the expection of the HH intermolecular Coulomb potential, the numerical details of the potentials are given in Tables 2 and 3. The Coulomb intermolecular HH potentials used in runs 2 and 3 are illustrated in Fig. 3. Other than for the cut-off distances, the potential functional forms were the same with $\alpha = 1$, $Q = 0.139$ e where e is the electron charge. The $Q = 0.139$ e value arises from requiring that, at equilibrium separation,

$$-D_e(OO) - D_e(OH) + \frac{Q^2}{R_e} = 5 \text{ kcal/mole.} \qquad (3)$$

The same value of Q is conceptually justified for use in both runs 2 and 3 by the fact that the value of Q, although sensitive to $D_e(OH)$ and $D_e(OO)$, is rather insensitive to the HOH spatial orientation relative to the $OHOH_2$ plane as shown by Morokuma and Pederson[12]. Indeed, that insensitivity can be viewed as a justification for modeling water in two dimensions.

TABLE 2

INTRAMOLECULAR MORSE POTENTIAL CONSTANTS*

RUN NO.	INTERACTION	D_e (eV)	$A_1(A^{-1})$	R_e (A)	R_c^a (A)
1	OH	5.1768	2.2188	1.01	3.5
	HH	0.5275	2.1920	1.01	3.5
2	OH	5.1768	2.2188	1.01	3.5
	HH	0.5275	2.1920	1.01	3.5
3	OH	5.1768	2.2188	1.01	2.3
	HH	0.5275	2.1920	1.4284	2.3

*Numbers to two or three significant figures (such as 2.3 and 1.01 are in reality followed by zeros (e.g., 2.30000...). All other listed numbers simply represent the first few signficant figures.

1 eV = 1.602×10^{-12} erg.

[a] R_c is the cut-off distance (i.e., for $R > R_c$ the potential is constant and the force vanishes).

TABLE 3

INTERMOLECULAR POTENTIAL CONSTANTS*

RUN NO.	INTERACTION	D_e (eV)	A_1 ($Å^{-1}$)	R_e (Å)	R_c^a (Å)
	OO	3.0350×10^{-2}	2.6626	2.76	4.5
1	OH	0.5692	10.094	1.75	2.05
	HH	0.5265	10.960	1.75	2.05
	OO	3.035×10^{-2}	1.3313	2.76 Å	4.5
2	OH	0.5181	2.2188	1.75	2.05
	HH	SEE TEXT AND FIGURE 3			2.05
	OO	3.035×10^{-2}	2.6626	2.76 Å	3.5
3	OH	0.5181	2.2188	1.75	2.3
	HH	SEE TEXT AND FIGURE 3			2.3

* See footnote to Table 2.

[a] See corresponding comment, Table 2.

All of the potentials used in these CMD runs contained a "damping" term which smoothed the potential in its approach to a constant value at the cut-off distance R_c. This was done in order to prevent a discontinuity in the forces at R_c. For example, run 1 utilized a damping function which led to a smoothed force, F_D, given by

$$F_D(R) = F(R) - F(R_c) \exp\left[-16\left(\frac{R_e}{R}\right)^3\left(\frac{R_c - R}{R_c - R_e}\right)^2\right] \quad (4)$$

where F(R) is the force derived from the undamped potential.

The magnitudes of the potentials for the different intermolecular interactions (all runs) at equilibrium (net equilibrium in the Coulomb interaction cases) are such that

$$|V(HH)| \approx |V(OH)| \sim 10|V(OO)| \quad (5)$$

While potential well depth is important for "chemistry" (e.g., bond breaking), the dynamics are controlled by the curvature of the potentials near equilibrium. For example, for a 0.1 Å displacement from equilibrium in the run 3 Coulomb-interaction case, the intermolecular-force magnitude ratios are given by (from Table 3 and Q = 0.139 e).

$$\frac{F(OO)}{F(HH)} = 2.7, \qquad \frac{F(OH)}{F(HH)} = 35. \quad (6)$$

The inter- and intramolecular forces must, of course, be related to known water inter- and intramolecular vibrational frequencies. From $F = -2D_eA_1^2(R-R_e)$, it is seen that near equilibrium a Morse potential is equivalent to a spring constant $K = 2D_eA_1^2$ with a corresponding frequency f (in inverse cm optical units) of

$$f = \frac{1}{2\pi c}\sqrt{\frac{2D_eA_1^2}{\mu}} \quad (7)$$

where c is the speed of light in vacuum. Using the reduced mass μ for OH in Eq. (7) gives, from Table 2, for the intramolecular OH interaction

$$f_{intra}(OH) = 3.9 \times 10^3 \text{ cm}^{-1} \tag{8a}$$

From Table 3 and with the reduced mass corresponding to the interaction of two water moleculars,

$$f_{inter}(OH) = 1.9 \times 10^3 \text{ cm}^{-1}, \text{ run 1} \tag{8b}$$

$$f_{inter}(OH) = 0.4 \times 10^3 \text{ cm}^{-1}, \text{ runs 2 and 3.} \tag{8c}$$

The Eq. (8a) result corresponds fairly closely to reality in that it is a frequency approximately equal to that associated with the water-vapor molecule symmetrical zero-order stretching mode (3825.3 cm^{-1})[14]. Eqs. (8b) and (8c) represent a hard shallow potential [from Table 3, 0.57 eV for Eq. (8b) and 0.52 eV for the Eq. (8c) cases]. There is no single piece of experimental evidence with which to compare the Eqs. (8b) and (8c) results in that, for example, the observed[16] (Raman spectra) intermolecular hydrogen bond stretching mode frequency of aproximately 200 cm^{-1} corresponds to the totality of potentials which, via their interaction, results in the "hydrogen bond" within the total water structure.

The physical effect of the hard [Eqs. (8b) and (8c)] intermolecular OH potentials used in these CMD runs is that OH bond breaking will occur for a smaller OH bond length change than, say, for a potential whose bond frequency is characterized by 200 cm^{-1}. The energy, however, for the proton to be raised out of its well (bond breaking) would be the same (0.5 eV) for either the Eq. (8B) and Eq. (8c) frequencies or for 200 cm^{-1}. However, as indicated earlier, under the pressures and densities characteristic of the shock front and the region behind the front, the potential barrier to proton transfer could be considerably reduced or eliminated when the presence of neighboring molecules is taken into account. This effect has not be considered in the present calculations but certainly should be included at a later stage.

Because, as seen from the Eq. (6) force ratios, the hardest intermolecular potential is associated with the OH bonding potential, it is possible to interpret the above paragraph in a shock-compression PdV language. There are two intermolecular OH bonds per molecule and approximately 3.5×10^{22} water-vapor molecules per cm^3. For our present pressure-independent intermolecular potentials, the 0.52 eV OH bonding wells are equivalent to a potential-energy pressure of approximately 58 kbar. Assuming that the shock pressure is equipartitioned between particle velocity and strain, one would

thus expect significant intermolecular bond breaking in these CMD runs in the vicinity of 120 kbar (as indeed observed in run 3). If the OH bond strength was softer and more competitive with, say, the OO intermolecular potential, then the above shock-pressure interpretation would be changed (to higher pressures) because an increased fraction of the total strain energy would then be going into the OO bonds+.

The 2.05 Å cut-off distance for the intermolecular HH potentials with the triangular structure is smaller than any initial inter-row HH separations. Thus, for the triangular structures (runs 1 and 2), molecular rotation transfer across molecular rows is expected to be inhibited - as indeed observed in the CMD results. On the other hand, the distance between atoms H_a and H_b in the Fig. 2 square lattice is less than the run 3 cut-off distance of 2.3 Å. Thus, for the square lattice one would expect to see a more uniform (row-to-row) molecular rotation distribution pattern than in the triangular lattice case; again, this is borne out in the CMD runs.

+ Because an OO bond is colinear with a very hard intramolecular OH bond plus a hard intermolecular OH bond, the OO and OH intermolecular bonds are subject to the same change in length for a compression along their common bond direction.

THE CMD RESULTS

Molecular dynamics has now evolved to a sophisticated level because of the dramatic revolution in large-scale computer technology. Simply stated, molecular dynamics involves the numerical solution by computer of Newton's equations of motion for all the atoms comprising the active region of the assembly. As a result, the coordinates and velocities of the particles are obtained as functions of time.

The force acting on any one particle in the ensemble is the resultant of all interactions with other atoms in its neighborhood. In principle, it should be obtained as the derivative of an effective many-body potential. However, any calculations which would, in fact, attempt to include most or all of a complete potential energy hypersurface would be far beyond present considerations. Fortunately, our experience, to date, indicates that much can be learned within the framework of the simple pair-potential approximation.

The set of coupled non-linear, second-order differential equations that represent the forces are reduced to a double set of first-order ordinary differential equations by standard procedures. The initial positions and velocities of the particles represent the initial conditions on these equations. For the numerical solution of this set of equations, we have employed the variable time-step, variable-order, implicit Adams'

method with functional (or fixed point) iteration, a generalization of the classical Adams-Bashforth-Moulton method[17]. The time step varied between approximately 5×10^{-19} sec and 5×10^{-16} sec depending upon the maximum acceleration of any atom within the array. Relative error buildup is controlled by an error tolerance parameter, so that numerical errors in the normalized velocities and positions are typically kept to less than one part in a million for times up to 10-50 picoseconds during a simulation. Symmetry checks are routinely made to verify the accuracy of error control.

One of the most striking features of these CMD runs is the occurrence of new dimer (and also higher-order) molecular arrangements such as $[O^{HH}_{HH}O]$ as can be clearly seen in Figs. 4 and 6. These molecular arrangements are occurring because the potentials used are strictly central and of the additive two-body type (i.e., the form of an OH potential is not influenced by an intervening H atom) and because the HH repulsion is weak relative to the strong intermolecular OH interaction.

The new water arrangements mentioned in the above paragraph are, of course, not realistic in that they are ruled out by the molecular orbital theory[18] of water-vapor molecular structure; theoretically, the OH potentials should not be the simple central potentials used here but should have the complicated angular dependence characterizing the lone-pair electron

wavefunctions[18]. Additionally, the Q value of 0.139 e resulting from Eq. (3) is approximately a factor of 1/3 the molecular orbital atomic-charge population prediction of Morokuma and Pedersen[12]. A larger Q value would have increased the intermolecular HH repulsion and made forming such new molecular arrangements more difficult.

At 100 kbar (run 3, Fig. 6), the shock energy associated with the thin flyer is quickly dissipated in breaking the intermolecular OH bonds with the result that a volume strain does not propagate into the sample much beyond 21 ticks. Yet, because of the energetically-favored above-mentioned new molecular arrangements, a rotational disturbance continues to propagate to the end of the target. While probably not found in real water, such rotational propagation effects are of considerable interest in themselves and could correspond to the diffusion of anisotropy perturbations (in the absence of strain) as treated by Leontovich[19] in his study of optical scattering.

At the 300 kbar level of runs 1 and 2, there is enough strain energy, even with the thin flyer, for the volume strain to propagate to the end of the (short) target and cause spallation. Additionally, the initial structures of runs 1 and 2 are not conducive to the new molecular arrangements as is run 3. The result is that in runs 1 and 2 the new arrangements occur only after sufficient time for the shock-induced

temperature to result in molecular orientation relationships favorable to the new dimer (and higher-order) phases.

The alternate row repeating rotational behavior observed in runs 1 and 2 is the result of impact symmetry and the already mentioned lack of HH interaction across the rows with the initial triangular structures. While in run 1 this repeating behavior has largely disappeared by the 38 tick frame, it is still very much in evidence in run 2 at 36 ticks. The reason for the temporal difference between runs 1 and 2 is that the Morse HH intermolecular interactions of run 1 are more favorable to the new molecular arrangements than the repulsive Coulomb interactions of run 2. The result is that these new molecular arrangements tend to form quickly in run 2 and, in the process of forming, they wash out the every-other-row rotational behavior.

The 75 tick run 3 frame of Fig. 6 is very interesting in that it appears that the high degree of symmetry perpendicular to the direction of shock propagation is beginning to thermalize to a (probably) more isotropic state characteristic of a liquid. This effect is most visible near the impact line. That a thermalization should begin to occur at 67 ticks (75 - 8) is in agreement with our present understanding[5] of a picosecond shock-front rise time in water to 100 kbar. While this thermalization time behavior is gratifying, it should be

viewed with some caution because our CMD structures and potentials do not quite duplicate real water.

The intermolecular OO potential was softened (see Table 3) in going from run 1 to run 2 in order to lower the shock velocity to a value more in keeping with experimental observation[9] for real water. While it is always possible for a given structure to duplicate bulk shock-wave properties by varying potential parameters, such duplication should not be taken as the mark of success in that many materials of differing molecular structure have very similar bulk shock-wave properties. In that regard, it is gratifying to observe expected changes in the intermolecular HH separation in all the runs. However, for the formation of complex ionic species at 300 kbar (runs 1 and 2), it is possible that we may require, in addition to a pressure-dependent lowering of the potential energy barrier for proton transfer, a period of time somewhat > 1 ps in order to have sufficient equipartitioning of energy among the molecular degrees of freedom. This is by no means certain, of course, and represents an area for further study.

CONCLUSIONS

Two-dimensional hydrogen-bonded structures of water-vapor molecules have been impacted under CMD conditions. In so far as the most important aspect of liquid water (or ice) is the intermolecular hydrogen bonding, we have performed CMD

shock-wave experiments on water (ice). There still, however, remains much to be done. Longer running times are necessary so that the details of thermalization can be investigated as a function of time and so that a supposedly picosecond shock-front rise-time can be viewed as an entity.

In order to have a model that can yield dissociation at 300 kbar, the O-H-----O potentials must be modified by first allowing for the presence of a double minima, then secondly permitting under shock loading the reduction or elimination of the potential barrier inhibiting proton transfer (e.g., due to density dependent proximity of neighboring molecules). Thus, the probability of forming positive ion species would be enormously enhanced. If, additionally, the simulations are then run to longer times in order to ensure thermalization (i.e., equipartition of the shock energy among the molecular degrees of freedom) and complex formation does not occur, a different interpretation of the saturating electrical conductivity may be necessary. Finally, the potentials must be modified to be more representative of the non-central lone-pair electron wavefunction distribution. That latter modification will probably be sufficient to prevent the peculiar molecular arrangements discussed in the previous section. While the various PVT phases of water are probably truly 3-dimensional in nature, at a later stage something also must be added within the

framework of our 2-dimensional physics approach to allow for phases which correlate with those of real water.

The small intermolecular HH interaction cut-off distance (2.05 Å in runs 1 and 2) should be increased to some value which is understood on the basis of real intermolecular interactions. If R_c were thus increased, the isolation of rotation between successive molecular rows would be diminished with perhaps a concurrent faster shock-front rise time. Such a lengthening of R_c would also be important to any ultimate CMD experiments attempting to duplicate shock-polarization experiments.

Much work remains to be done.

ACKNOWLEDGEMENTS

Work performed under the auspices of the U. S. Department of Energy by the Lawrence Livermore National Laboratory under contract number W-7405-ENG-48 and the Office of Naval Research under contract E00014-84-F-0094.

Both authors are indebted to T. DeBoni (LLNL) for enthusiastically carrying out the CMD runs discussed in this report. One of the authors (PH) also acknowledges the helpful discussion of H. N. Presles of the Univ. of Poitiers (France).

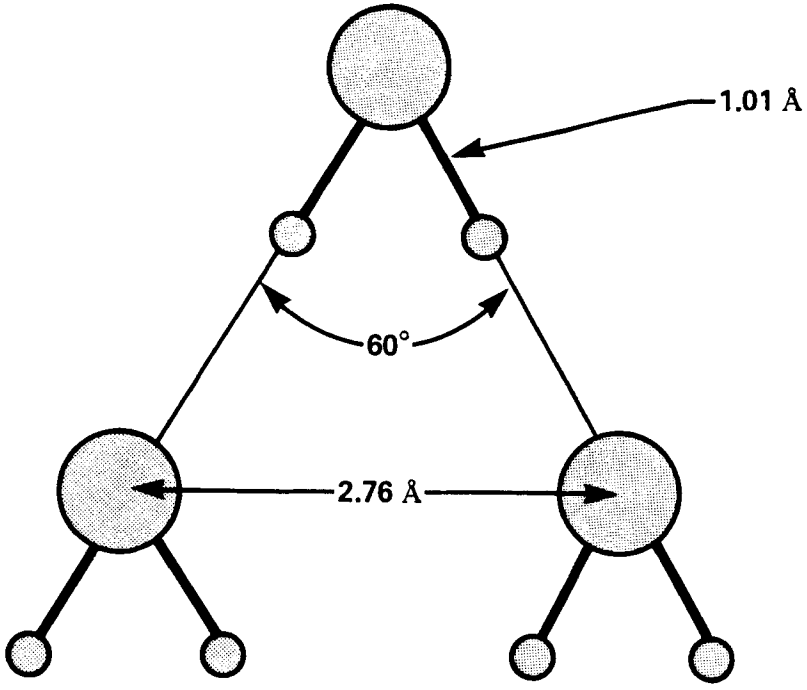

FIGURE 1

Initial triangular lattice structure. Large circles are oxygens and small circles are hydrogens.

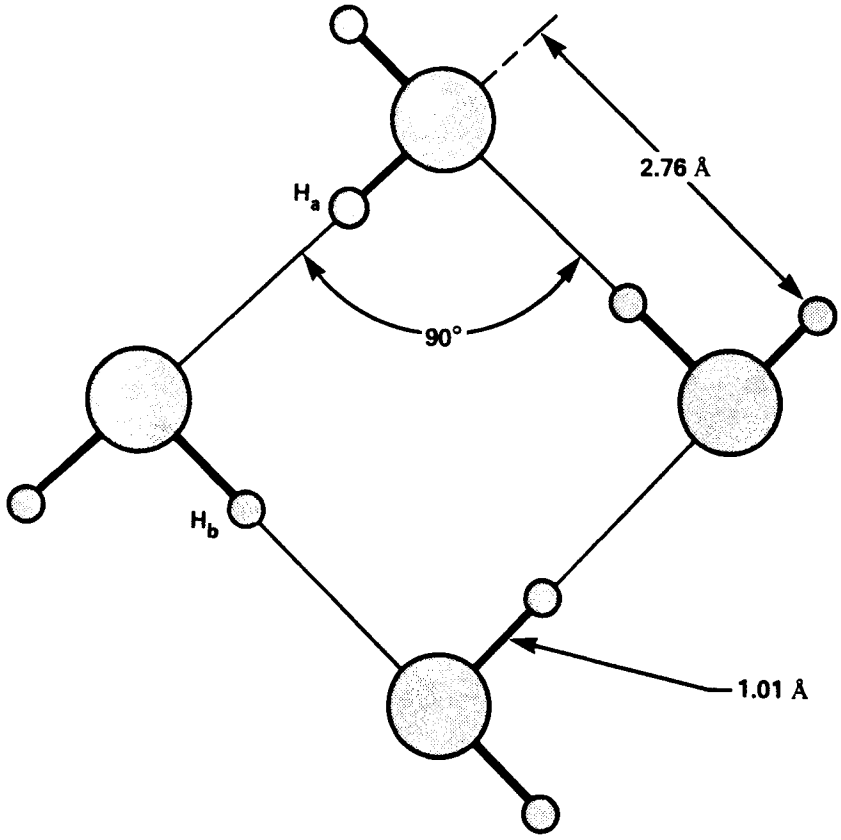

FIGURE 2

Initial square lattice structure. Large circles are oxygens and small circles are hydrogens. The hydrogen atom labels H_a and H_b are for purposes of discussion within the text.

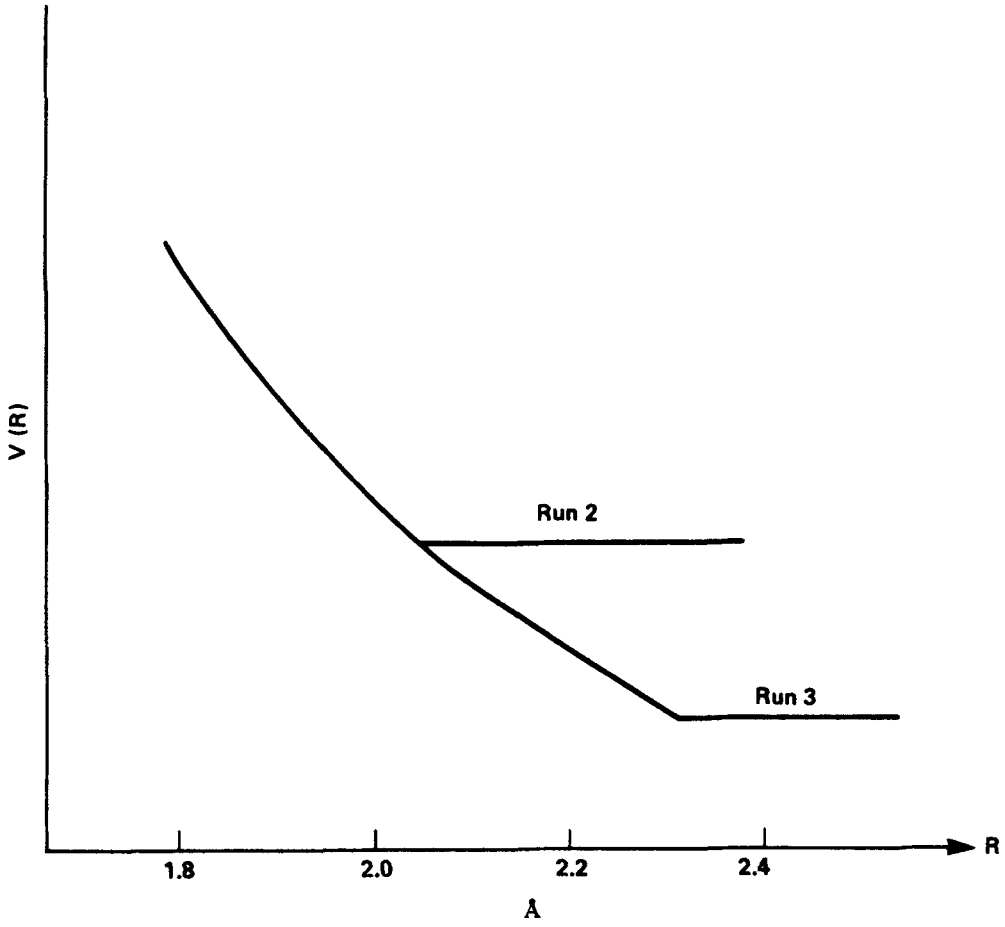

FIGURE 3

Coulomb potential for runs 2 and 3. The cut-off for run 2 is R_c = 2.05 Å and for run 3 is R_c = 2.3 Å.

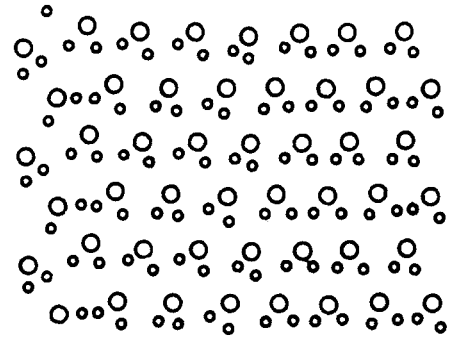

12 ticks

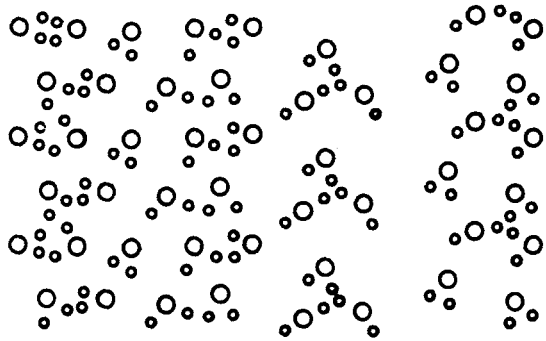

26 ticks

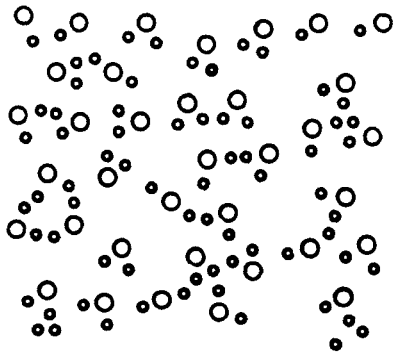

38 ticks

FIGURE 4

CMD run 1. Impact occurs at approximately 8 ticks. The impacting plate enters from the left and is composed of 4 columns of 3 molecules per column. Free surface spall has already occurred at 26 ticks with the spalled layer being off screen by 38 ticks. Unconnected hydrogens are not unbonded but have simply been reflected across the transverse periodic boundaries. Notice the approximate every-other-row repeating pattern of rotational behavior to 26 ticks. One tick = 10^{-14} sec.

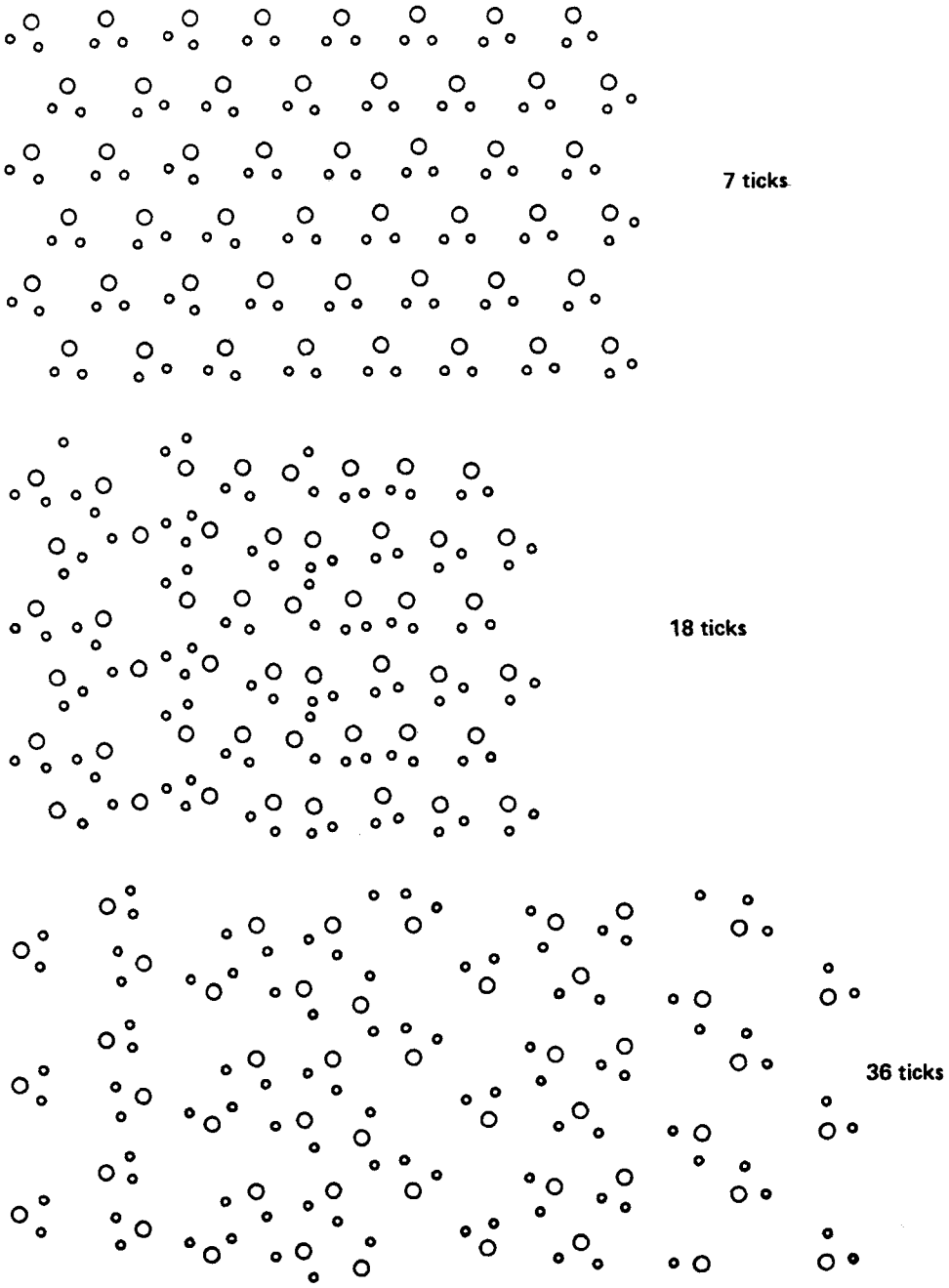

FIGURE 5

CMD run 2. Impact occurs at approximately 7 ticks. Again, the impacting plate enters from the left and is composed of 4 columns of 3 molecules per column. Spall layer separation at the free surface is just beginning to occur at 36 ticks. Again, notice the approximate every-other-row repeating pattern of the rotational behavior, but now to 36 ticks. One tick = 10^{-14} sec.

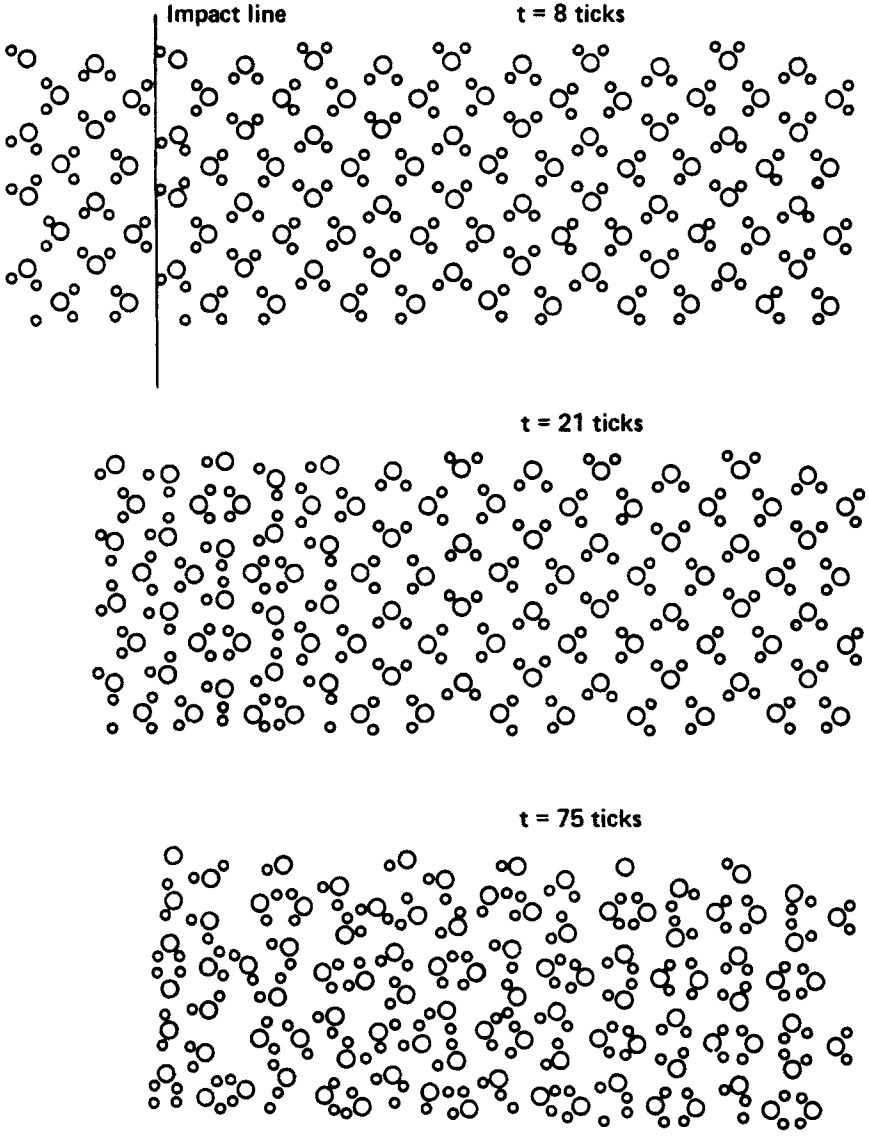

FIGURE 6

CMD run 3. Impact is just occurring at 8 ticks. Impacting plate enters from the left and is composed of 4 columns of 4 molecules per column. Notice the rotational behavior and the peculiar water dimer arrangements. One tick = 10^{-14} sec.

REFERENCES

1. K. Niki and S. Ono, Physics Letters 62A, 427 (1977).
2. A. N. Dremin and V. Yu. Klimenko, Progress in Astronautics and Aeronautics 75, 253 (1979).
3. B. L. Holian, W. G. Hoover, B. Moran, and G. K. Straub, Phys. Rev. A 22, 2798 (1980).
4. D. Tsai and S. Trevino, Phys. Rev. 24, 2743 (1981).
5. P. Harris and H. N. Presles, J. Chem. Phys. 77, 5157 (1982).
6. P. Harris and H. N. Presles, J. Energetic Materials 1, 45 (1983).
7. P. Harris and H. N. Presles, J. Chem. Phys. 80, 524 (1984).
8. F. H. Stillinger and A. Rahman, J. Chem. Phys. 60, 1545 (1974).
9. M. H. Rice and J. M. Walsh, J. Chem. Phys. 26, 824 (1957).
10. A. C. Mitchell, M. I. Kovel, W. J. Nellis, and R. N. Keeler in High Pressure Science and Technology, Vol. 2, B. Vodar and Ph. Marteau, editors (Permagon Press, Oxford, 1969).
11. See, for example, M. Eigen, Angewandte Chemie 3, 1 (1964).
12. K. Morokuma and L. Pedersen, J. Chem. Phys. 48, 3275 (1968).

13. For a discussion of some of the possible results of employing periodic boundary conditions in CMD programs see, for example, H. C. Anderson, J. Chem. Phys. 72, 2384 (1980).

14. D. Eisenberg and W. Kauzmann, The Structure and Properties of Water (Oxford Univ. Press, Oxford, 1969).

15. F. H. Stillinger, Science 209, 451 (1980).

16. G. E. Walrafen, J. Chem. Phys. 40, 3249 (1964).

17. C. W. Gear, Numerical Initial Value Problems in Ordinary Differential Equations (Prentice-Hall, Englewood Cliffs, New Jersey, 1971), Chapter VII.

18. J. A. Pople, Proc. Roy. Soc. A 202, 223 (1950).

19. M. Leontovich, J. Phys. (USSR) 4, 499 (1941).